

Modeling of Synchronized Bursting Events: The Importance of Inhomogeneity

Erez Persi

erez.persi@biomedicale.univ-paris5.fr

David Horn

horn@post.tau.ac.il

Vladislav Volman

hamlet@tamar.tau.ac

Ronen Segev

rsegev@molbio.princeton.edu

Eshel Ben-Jacob

eshel@tamar.tau.ac.il

School of Physics and Astronomy, Raymond and Beverly Sackler Faculty of Exact Sciences, Tel-Aviv University, Tel-Aviv 69978, Israel

Cultured *in vitro* neuronal networks are known to exhibit synchronized bursting events (SBE), during which most of the neurons in the system spike within a time window of approximately 100 msec. Such phenomena can be obtained in model networks based on Markram-Tsodyks frequency-dependent synapses. In order to account correctly for the detailed behavior of SBEs, several modifications have to be implemented in such models. Random input currents have to be introduced to account for the rising profile of SBEs. Dynamic thresholds and inhomogeneity in the distribution of neuronal resistances enable us to describe the profile of activity within the SBE and the heavy-tailed distributions of interspike intervals and interevent intervals. Thus, we can account for the interesting appearance of Lévy distributions in the data.

1 Introduction

How an ensemble of neurons links together to form a functional unit is a fundamental problem in neuroscience. The difficulty in visualizing and measuring the activity of *in vivo* neuronal networks has accelerated the tendency to pursue surrogate methods. As a result, much effort has been devoted to studying cultured neuronal networks *in vitro*. It has been suggested (Marom & Shahaf, 2002; Shahaf & Marom, 2001) that large, random networks *in vitro* are probably the most appropriate experimental model to study the formation of activity of groups of neurons and the response of this functional connectivity to stimulation. Unlike *in vivo* networks, ran-

domly formed in vitro networks are free of any predefined functional role and enable one to study how a system self-organizes.

Many different forms of synchronized activity of populations of neurons have been observed in the central nervous system (CNS) through the years. However, the role of synchronization in the neural code and information processing is still a matter of considerable debate. Recently, Segev et al. (2001) and Segev, Shapira, Benveniste, and Ben Jacob (2001) performed long-term measurements of spontaneous activity of in vitro neuronal networks placed on multielectrode arrays. These developing networks show interesting temporal and spatiotemporal properties on many timescales. At early stages (up to a week), the neurons spike sporadically, after which they begin to correlate, leading to the emergence of synchronized bursting events (SBEs). An SBE involves extensive spiking of a large fraction of neurons in the system during approximately 100 msec. One hypothesis (Segev, 2002) is that these dynamic SBEs are the substrate for information encoding at the network level, in analogy with action potentials at the neuronal level.

Different morphological structures and sizes of networks were explored (Segev, Benveniste, et al., 2001). All networks exhibit (1) long-term correlation of the SBEs' time sequence manifested by power law decay of the power spectrum density, (2) temporal scaling behavior of neuronal activity during the SBEs (where most of the activity takes place), and (3) temporal scaling behavior of the SBEs' time sequence. Temporal scaling is usually expressed by a power law decay. The time sequences of spikes and SBEs were well fitted to a Lévy distribution, which has a power law decay. Such scale-invariant behavior is characteristic of dynamical systems, which are composed of many nonlinear components (Mantegna & Stanley, 1995; Peng et al., 1993).

Our goal is to elucidate the underlying mechanisms and properties of the different elements in the system responsible for the generation and structure of the observed neuronal (synchronized) activity.

2 Experimental Observations

The experimental system is based on a two-dimensional (2D) 60-multi-electrode array on which the biological system is grown. The biological system is composed of both neurons and glia, taken from the cortex of a baby rat. The coupling between the electrodes and the neuronal membranes enables the recording of neuronal electric activity (action potentials). Different morphological types and sizes of networks were explored (Segev, Benveniste, et al., 2001): (1) quasi one-dimensional (1DS), a small network composed of 50 cells; (2) rectangular (2DM) a medium-sized network composed of 10^4 cells; and (3) circular (2DL), a large-size network composed of 10^6 cells. All of these networks shared the same characteristic patterns of activity. The mean rate of SBEs increases with the size of the network, while the variance decreases, but only up to a factor of 2.

2.1 Synchronized Bursting Events. Figure 1 illustrates a characteristic raster plot, revealing the appearance of SBEs and their structure. The SBE involves rapid spiking of almost all the neurons in the network. It starts abruptly and decays during a 100 msec period. During the SBE, each neuron has its own firing pattern, consisting of up to 20 spikes. The SBEs are separated by long quiescent periods (1–10 sec) during which there is almost no activity except for a few sporadic spikes. The mean rate of SBEs is between 0.1 Hz and 0.4 Hz.

2.2 Distribution of Neuronal Activity. The distributions of ISI at the neuron level, and interevent interval (IEI) at the network level were analyzed (Segev, Benveniste et al., 2001). Since the SBE width is of the order 100 msec, this defines the resolution of IEIs. The ISI and IEI distributions of experimental data reveal heavy tails, indicating possible temporal scaling behavior. To study the appearance of heavy tails in ISI and IEI, the distributions of the ISI and IEI increments, defined by

$$\Delta ISI(t) = ISI(t) - ISI(t - 1) \quad (2.1)$$

$$\Delta IEI(t) = IEI(t) - IEI(t - 1), \quad (2.2)$$

were investigated. Unlike the ISI and IEI, the increments have symmetric stationary distributions with zero mean. Figure 2 displays the histograms of the ISI increments of three different neurons, as well as the average of all experimental data and the margin of variation. We note that since the activity is very low between any two consecutive SBEs, the first part of the histogram (up to 100 msec) is separated from the second part (from 2 sec), which reveals the heavy-tailed distribution of the IEI increments (since ISI increments larger than 1–2 sec are caused mainly by the SBEs). Between 100 msec and 2 sec, the probability increases slightly for each neuron due to both the synchrony and sporadic activity in the system. We also calculate the distance between the individual neurons' histograms and the averaged histogram using the KL divergence measure defined by:

$$D_{KL} = \sum_x P(x) \cdot \log_2(P(x)/Q(x)). \quad (2.3)$$

The values are given in the figure caption. These values will be compared later with model neurons.

Since these distributions exhibit large tails, it seems only natural to try to fit them by Lévy distributions, which would also be expected from central limit theorem arguments (see below). In this article, we follow the parameterization $S(\alpha, \beta, \gamma, \delta; 0)$ (Nolan, 1998, 2004) to describe Lévy distribution.

Every Lévy distribution is a stable distribution. A random variable X is stable if $X_1 + X_2 + \dots + X_n \sim C_n X + D_n$, meaning that the normalized

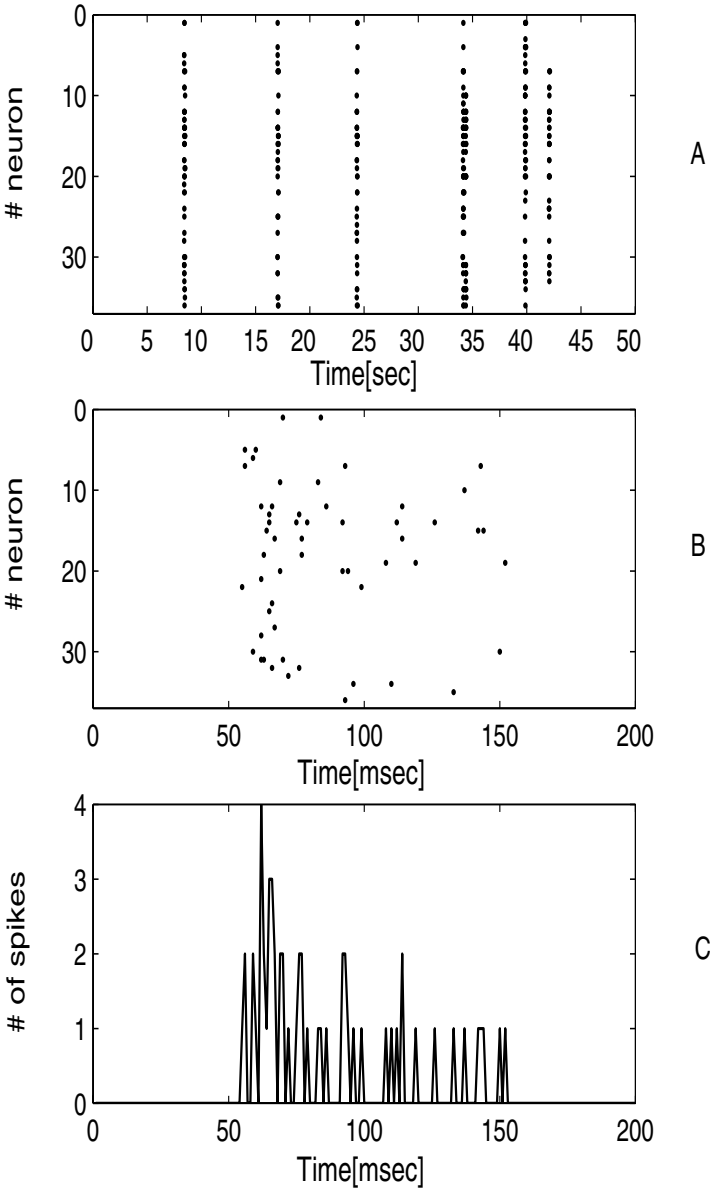


Figure 1: Typical activity of the experimental network. (Top) The raster plot of 1 msec time bins reveals SBEs. (Middle) Zoom into an SBE. (Bottom) Detailed structure of an SBE, displayed by the number of spikes in the network per time bin.

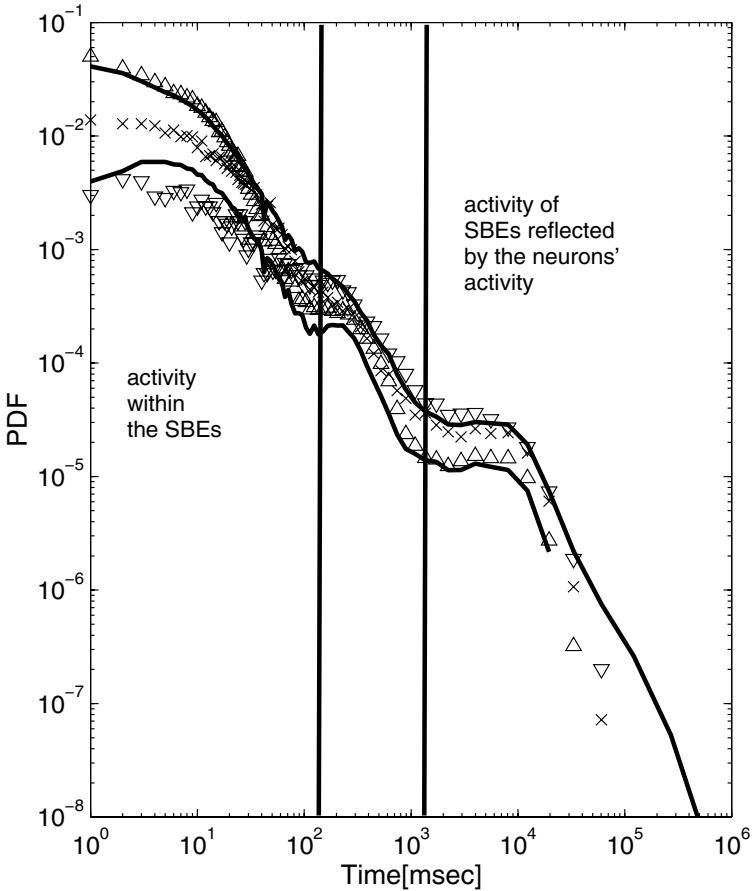


Figure 2: Positive half of the neurons' Δ ISI histograms, taken from the experimental data. Solid lines represent the margins of variability. They are calculated by averaging the histograms of all neurons and plotting this averaged PDF \pm the standard deviation. Symbols represent data of three selected neurons, also showing the diversity in the data. The KL distance measures of these neurons from the average PDF are $4.1193 \cdot 10^{-6}$, $3.1369 \cdot 10^{-6}$, and $3.1355 \cdot 10^{-5}$, ordered according to the order of the neuron values at Time = 1 from top to bottom.

sum of independent and identically distributed (i.i.d.) random variables is also distributed as X , with a scaling factor $C_n = n^{1/\alpha}$ and a shift D_n . For the data in Figure 2, we find that Δ ISI distributions are well fitted with a Lévy distribution $S(\alpha, 0, \gamma, 0; 0)$ up to 100 msec, while Δ IEIs are well fitted with Lévy over another three decades. $0 < \alpha \leq 2$ is the index of stability, which

determines the long tail of the distribution, and $\gamma > 0$ is a scale factor, which determines the location of the bending point (see the examples in Figure 3). Special cases of the Lévy distributions are the gaussian distribution ($\alpha = 2$) and the Cauchy distribution ($\alpha = 1$). All $\alpha < 2$ have divergent variance.

There are several important properties of Lévy distributions worth pointing out. (1) The generalized central limit theorem (Nolan, 2004) states that the normalized sum of i.i.d. variables converges to a Lévy distribution. If the variance is finite, then $\alpha = 2$; the convergence is to a gaussian distribution. Otherwise, $\alpha < 2$. (2) If $\alpha < 1$, the mean is infinite too. (3) For $\alpha < 2$, the asymptotic behavior of the distribution is given by a power law $f(|X|) \propto |X|^{-(1+\alpha)}$.

In Figure 3, we present examples of different Lévy distributions plotted on log-log scales of the type used in Figure 2. This should help develop the understanding that γ replaces the SD parameter, specifying when the bending of the PDF occurs on the log-log plot. α determines the slope of the long tail. Since there are no closed forms for these stable distributions (except for particular cases), we use numerical simulations and display histograms instead of analytic distribution functions.

The observed behavior of ΔISI and ΔIEI implies that their variances diverge; there is no characteristic timescale in the system. Previous models of IF neurons with dynamic synapses were unable to account for these heavy-tailed distributions (Segev, Benveniste, et al. 2001). Our aim is to suggest mechanisms that will generate distributions of the kind observed experimentally.

3 The Model

Our model is based on leaky integrate-and-fire (IF) neurons endowed with frequency-dependent synapses (Markram & Tsodyks, 1996). An IF neuron captures the most important aspects of neuronal behavior: the integration of inputs during the subthreshold period and the generation of a spike once the threshold is reached. The IF neuron is described by

$$\tau_{mem} \cdot \frac{dv}{dt} = -v + R_{mem} \cdot (I_{syn} + I_{ext}), \quad (3.1)$$

where v , τ_{mem} , and R_{mem} are the voltage, time constant, and resistance of the cell membrane, respectively. Once v reaches a threshold, the neuron fires, and v is being reset to v_{res} .

Neural networks composed of IF neurons are able to generate bursting activity (Tsodyks, Uziel, & Markram, 1999) in a model based on frequency-dependent synapses. The phenomenological model of dynamic synapses was shown to accurately predict the behavior and properties of various neocortical connections (Markram, Pikus, Gupta, & Tsodyks, 1998; Tsodyks, Pawelzik, & Markram, 1998). The strength of a synapse is described by a

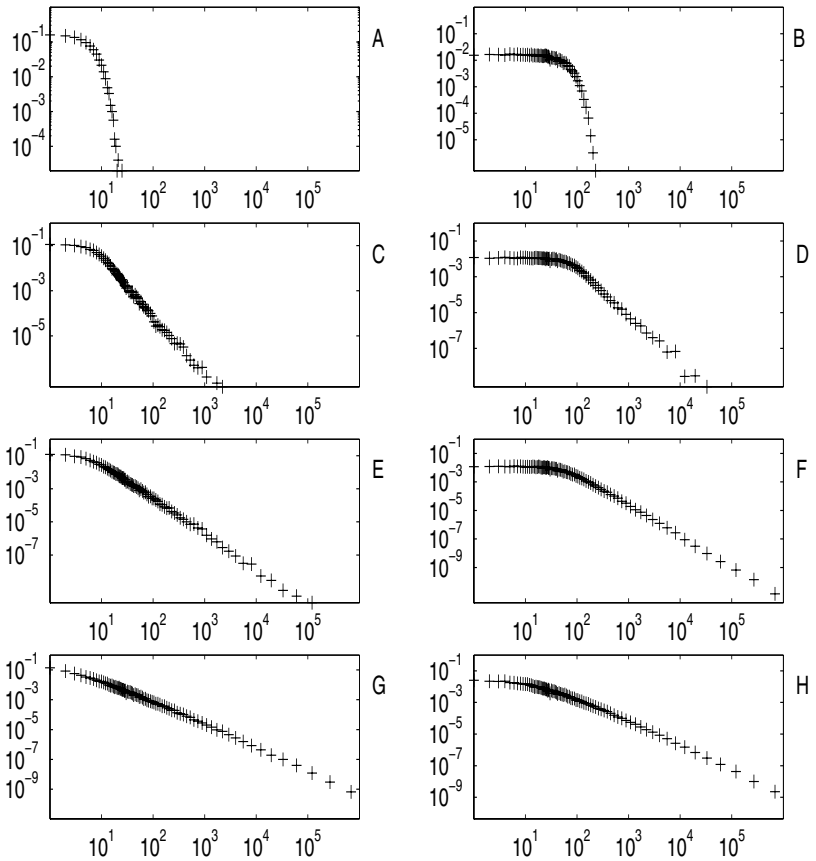


Figure 3: Examples of the positive half of gaussian and Lévy distributions on a logarithmic scale. (First row) Gaussian distributions with SD = 5 (left) and SD = 50 (right). Notice that increasing the variance shifts the bending point to the right but does not affect the asymptotic behavior of the distribution. (Second row) Lévy distributions with $\alpha = 1.5$, $\gamma = 5$ (left), and $\gamma = 50$ (right). Notice the slow convergence to zero of the tails. (Third row) Lévy distributions with $\alpha = 1.05$, $\gamma = 5$ (left), and $\gamma = 50$ (right). (Fourth row) Lévy distributions with $\alpha = 0.5$, $\gamma = 5$ (left), and $\gamma = 50$ (right).

parameter A_{ij} , representing the efficacy of a synapse connecting a presynaptic neuron (j) to a postsynaptic neuron (i). The dynamics of the synapse is described by the following system of differential equations:

$$\frac{dx}{dt} = \frac{z}{\tau_{rec}} - u \cdot x \cdot \delta(t - t_{sp}) \tag{3.2}$$

$$\frac{dy}{dt} = -\frac{y}{\tau_{ina}} + u \cdot x \cdot \delta(t - t_{sp}) \quad (3.3)$$

$$\frac{dz}{dt} = \frac{y}{\tau_{ina}} - \frac{z}{\tau_{rec}}, \quad (3.4)$$

where x , y , z are state variables representing the fraction of ionic channels in the synapse in the recover, active, and inactive states, respectively, with $x+y+z = 1$. u represents the fraction of utilization of the recover state by each presynaptic spike. Once a spike from a presynaptic neuron arrives at the synaptic terminal at time t_{sp} , a fraction u of the recover state is transferred to the active state, which represents the fraction of open ionic channels through which neurotransmitters can flow. The synaptic current from all presynaptic neurons to the postsynaptic neuron is therefore

$$I_{syn}^i = \sum_{j=1}^n A_{ij} \cdot y_{ij}. \quad (3.5)$$

After a short time τ_{ina} , the ionic channels switch into the inactive state. From the inactive state, there is a slow process of recovery ($\tau_{rec} \gg \tau_{ina}$) back to the recover state, completing a cycle of synapse dynamics. The above description (with a constant variable u) captures well the dynamics of a depressing synapse. The variable u describes the effective use of synaptic resources and could be assigned to the probability of release of neurotransmitters. In facilitating synapses, each presynaptic spike increases the probability of excreting neurotransmitters to the synaptic cleft. In order to capture the dynamics of facilitating synapses, another equation was added to the model:

$$\frac{du}{dt} = -\frac{u}{\tau_{fac}} + U \cdot (1 - u) \cdot \delta(t - t_{sp}), \quad (3.6)$$

where the constant parameter U determines the increase in the value of u each time a presynaptic spike arrives. The initial condition is that $U = u$. Note that when τ_{fac} approaches zero, facilitation is not exhibited. When a presynaptic spike arrives, u is updated first and then all other parameters (x , y , z).

Tsodyks et al. (1999) have demonstrated that a network of IF neurons with dynamic synapses of the type described above generates synchronized bursts. Their network was composed of 400 excitatory neurons and 100 inhibitory neurons with probability of 0.1 for connection between two neurons. Each postsynaptic excitatory neuron is connected to a presynaptic neuron through a depressing synapse, while each postsynaptic inhibitory neuron is connected through a facilitating synapse. The network is partially balanced—on average $3 \cdot A_{EE} = A_{EI}$, but $A_{IE} = A_{II}$. The network was fed a fixed external input current I_{ext} that was generated by a random flat distribution centered at firing threshold (with a range of 5% of the threshold).

The rate of SBEs obtained with this description is approximately 1 Hz. After an SBE occurs, it fades away rapidly since the fast firing neurons with depressing connections cause a sharp decline of recovering synapses. Between SBEs, there is a low-rate activity that enables the recovery of synapses, so I_{syn} builds up and leads to a new burst. The choice of parameters is given in the appendix.

Trying this approach on our system, we find that it needs modifications. It is difficult to find parameters that fit both the rate of SBEs and the low firing rate of neurons in between SBEs. Moreover, the profile of the experimental SBE—the activity of neurons within this event—rises sharply and decays exponentially, while the model as described so far leads to a narrow (20 msec) gaussian profile. The modifications that we propose are discussed in the next section.

4 Importance of Noise, Inhomogeneity, and Dynamic Thresholds _____

Here we investigate three modifications of the model. We add noise to the input current, introduce inhomogeneity into the resistances, and add dynamic thresholds that are also inhomogeneously distributed. The simulations reported below were performed on a network of 27 excitatory and 3 inhibitory neurons with 25% connectivity. For simplicity, we chose V_{th} and V_{res} to be 1 and 0, respectively, and $\tau_{mem} = 10$ msec. Since τ_{ina} determines the decay of synaptic currents that dominate during the SBE, we increased τ_{ina} to 10 msec. This leads to wide bursts of order 100 msec.

The biological system is grown on top of a biochemical substrate. Therefore, the neurons in the dish are subjected to sustained changes in the concentration of different substances that compose the external environment of the neurons. (For more details on the experimental methods, see Segev 2002 and Segev, Shapira et al., 2001.) In addition, each neuron (in the large networks) receives thousands of noisy synaptic inputs. We introduce external noisy current in our model in order to account for all these effects, as well as other hidden biological mechanisms, on both the neuronal and the synaptic levels. The external noise is chosen to be gaussian with an expectation value of $\mu = 0.86$ and standard deviation of $\sigma = 0.15$. Each 10 time steps (of 0.1 msec each), a different value of the external current is used. This leads to both quiescence between successive SBEs and a sharp increase in neuronal activity once an SBE starts, as shown in Figure 4.

Since μ is below threshold, the neurons' firing rate is very low. This enables the synapses to recover quickly and almost completely before the next SBE. At the point where the synapses are recovered, a single spike from one of the neurons in the network generates a large I_{syn} in its targets, thus increasing the probability of generating an SBE. When the SBE fades away, the synapses are in the inactive state, hence, the only activity is the one driven by the noisy external currents. The expectation value and variance of the noise control the mean rate of SBEs, which can be adjusted to fit the

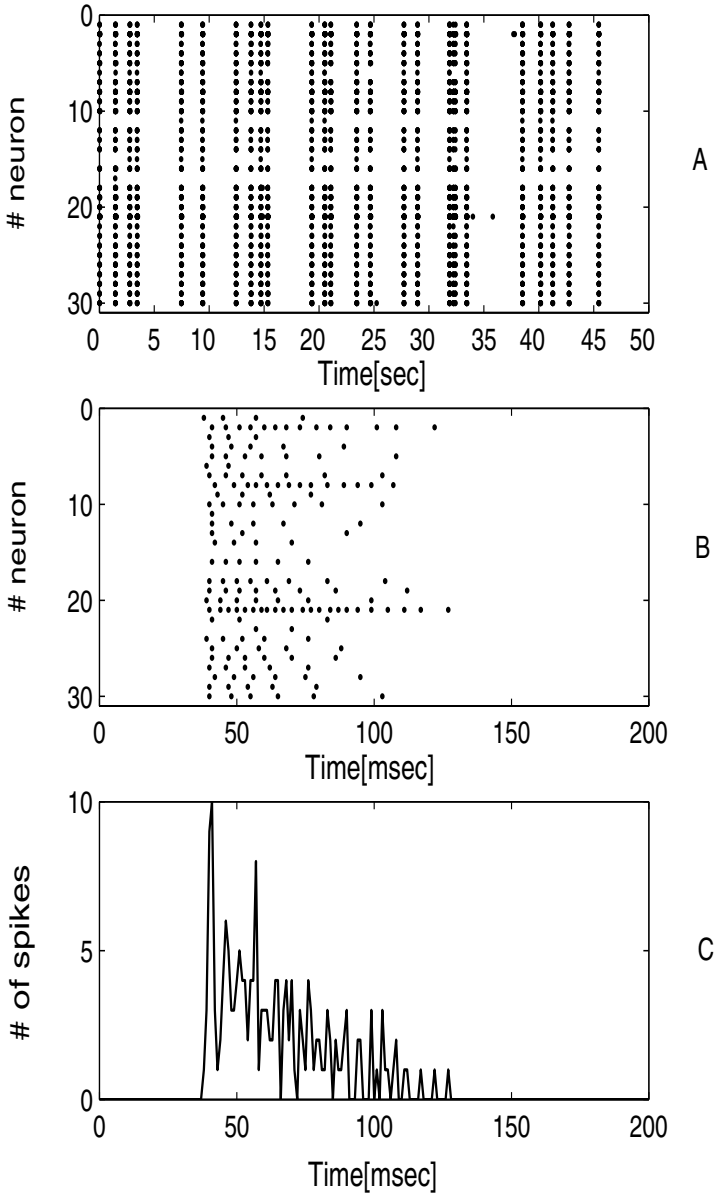


Figure 4: The bursting profile due to noisy external currents. (Top) Raster plot shows the quiescence between SBE. (Middle) Zoom into the SBE at 20 sec. The SBE width is 100 msec. (Bottom) The activity during SBE has the right profile but is too intensive.

experimental values. However, the profile of the simulated SBE builds up too fast in comparison with experiments. The ΔISI distribution possesses a heavy tail (power law behavior up to 100 msec), but it does not fit a Lévy distribution. This is a direct result of high activity during the SBE, since the probability of large ΔISI during the SBE is too low.

To cure these problems, we introduce inhomogeneity into the system. We start with inhomogeneity in neuronal resistances, the R_{mem} parameters of eq. 2.3. We select them randomly from a flat distribution over the interval $[0.1, 0.4]$. This modifies each neuronal I_{syn} , and the correlations between the activity of neurons during the SBE are weakened, leading to a slower SBE buildup. Since $I_{syn} \sim A_{ij}$, this is actually a rescaling of synaptic strengths. The resulting SBE perfectly matches the observed spatiotemporal structure (see Figure 5). Moreover, this choice leads to a Lévy distribution in ΔISI up to 50 msec, which suggests that the system still lacks a mechanism that allows the probability for large ΔISI to increase.

Next, we introduce dynamic thresholds in order to improve the Lévy distributions of ΔISI and ΔIEI . Adaptation and regulation are well-known characteristics of neuronal activity. It may be represented by dynamical thresholds, allowing for fatigue to set in upon receiving strong stimulation over long periods. For recent discussions of these effects, see Horn & Usher, 1989; Horn & Opher, 2000; Ying-Hui & Wang, 2000; Brandman & Nelson, 2002. Here we introduce dynamic thresholds that change as a function of the neuronal firing rate:

$$\frac{d\theta_i}{dt} = -\frac{\theta_i - \theta_i(t=0)}{\tau_{th}} + \eta_i \cdot \delta(t - t_{sp}). \quad (4.1)$$

θ describes the change in threshold, η_i is a factor chosen from a flat distribution over the interval $[-0.05, +0.05]$, and τ_{th} equals the SBE time width (100 msec), consistent with biological data. Note that our choices for η_i mean that there are two kinds of neurons, with thresholds that increase or decrease during an SBE. In other words, one kind of neuron displays fatigue while the other displays facilitation. Using this description, we obtain a good match (over five decades) to the probability distribution functions of ΔISI and ΔIEI and to the experimental spatiotemporal structure of SBEs, as demonstrated in Figures 5 and 6.

The fit to ΔIEI is interesting. Note that with homogeneous synaptic strengths, refractory periods, membrane time constant, and so forth, the probability of generating an SBE is determined by the time-varying external inputs and the specific connectivity of the network. This leads to a periodic-like SBE behavior as in Tsodyks et al. (1999). By allowing slight dynamical changes in these parameters, we are able to generate aperiodic behavior with long periods of quiescence, resulting in a Lévy distribution. The choice of parameters is given in the appendix. τ_{mem} and τ_{ref} are selected from flat distributions. This enables us to limit the dispersion of the selected

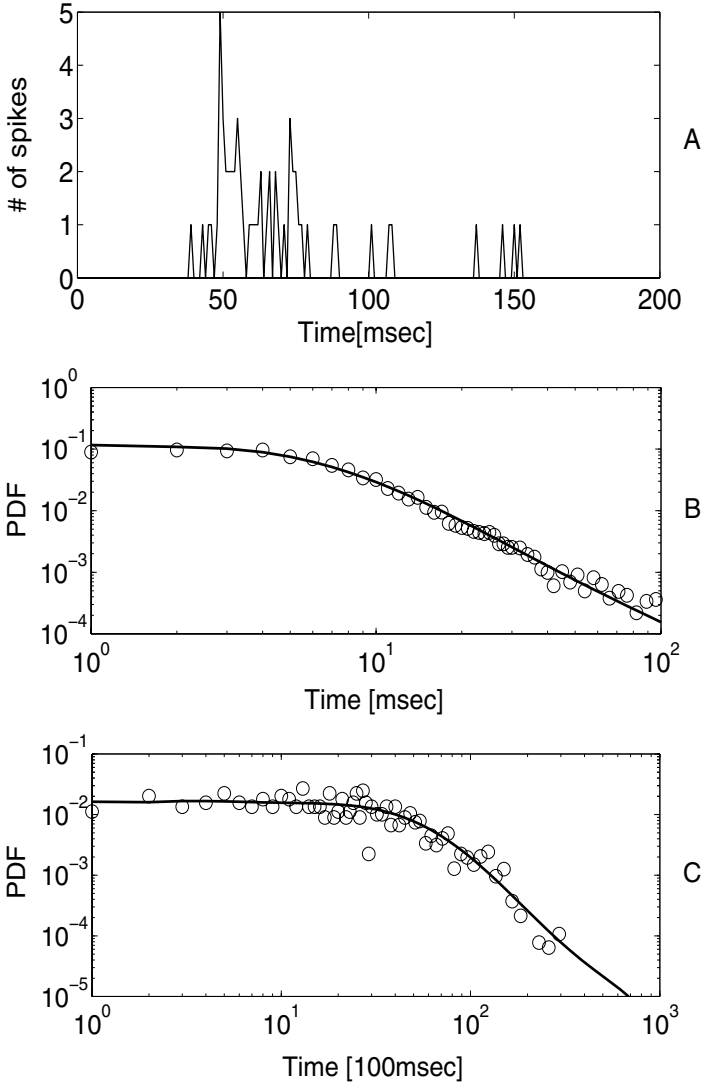


Figure 5: Effect of dynamic thresholds and inhomogeneous resistances. (Top) The SBE profile is similar to the experimental one (see Figure 1). (Middle) Circles represent the averaged histogram of Δ ISI histograms of all the simulated neurons. An averaged value is obtained for each time bin. The solid line is a computer-generated Lévy histogram with $\alpha = 1.25$, $\gamma = 5$. Fits to the data followed the maximum likelihood method of (Nolan 2001). The temporal resolution of spikes is set at 1 msec. (bottom) Circles represent the histogram of the simulated Δ IEI time sequence. The solid line is a computer-generated Lévy histogram ($\alpha = 1.6$, $\gamma = 25$). The temporal resolution of SBEs is 100 msec.

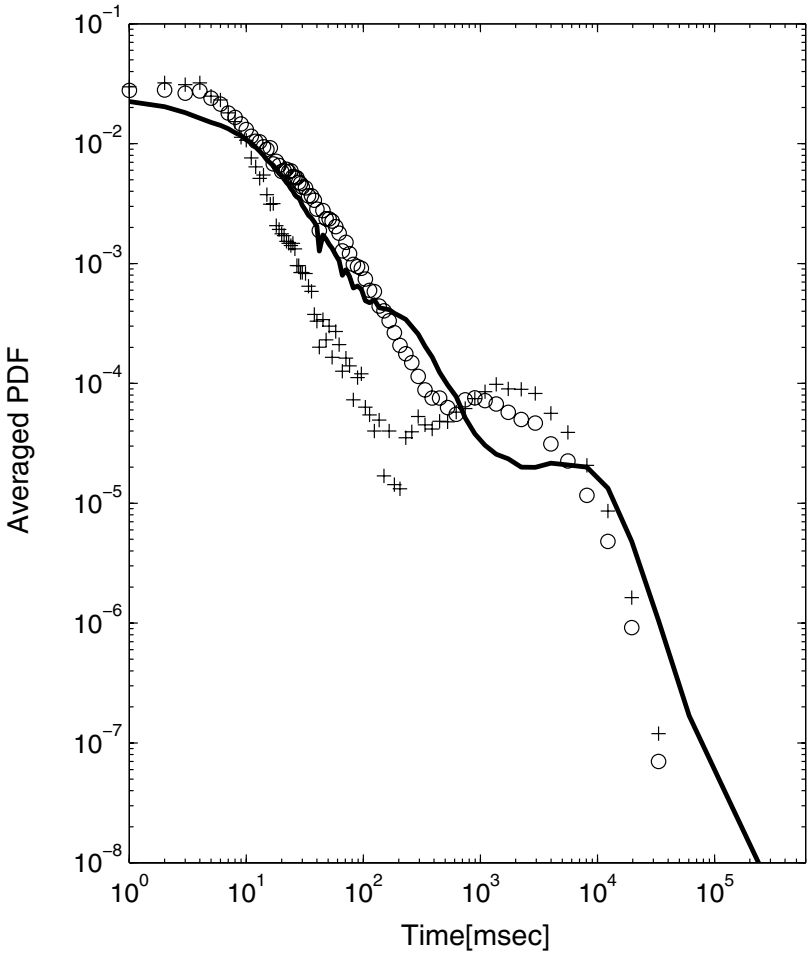


Figure 6: Effect of τ_{th} on the model for ΔISI . Solid curve: The averaged histogram of all the neurons of the experimental system (same data as in Figure 2). Symbols: Averaged histograms calculated from the results of the simulation. (+) curve $\tau_{th} = 100$ msec. (o) curve: $\tau_{th} = 450$ msec $\alpha \simeq 0.8$, $\gamma \simeq 20$. Note that τ_{th} affects mainly the slope of the histogram. The KL distance measure between these two models and the averaged experimental histogram are $D_{KL}(+) = 9.5695 \cdot 10^{-6}$, $D_{KL}(o) = 2.5147 \cdot 10^{-7}$.

values of the resistances but is not crucial to obtain the effects we already discussed.

5 Testing the Model

5.1 Sensitivity to Choice of Parameters. To gain further understanding of the model, we test its sensitivity to different parameters. The ratio of the number of excitatory to inhibitory neurons affects the rate and the shape of SBEs. Increasing the number of inhibitory neurons decreases the probability of generating SBEs. Moreover, strong inhibition decreases the activity of neurons during an SBE, resulting in a very dilute event. In the absence of inhibition (i.e., in an excitatory network), the network operates in an asynchronous mode, without generating SBEs. However, decreasing synaptic strengths ten-fold, the network reduces its total activity, and SBEs appear. This effect was referred to in Tsodyks et al. (1999). Reducing synaptic strengths further, the SBEs are still obtained, but their profile becomes symmetric.

The synaptic strengths (or resistances) determine the shape of the distributions. When A_{ij} is reduced by the same factor for all synapses attached to a postsynaptic neuron, the activity during an SBE is less dense (small I_{syn}), and the density of SBEs is reduced. This results in an increase of both γ (the bending point) and α (the long-tail decay) of the Lévy distribution of ΔISI . The effect on the shape of the ΔIEI distribution is very weak. There is a limit to our ability to control the shape of the distributions. Reducing the synaptic strengths leads to a low activity rate with symmetric SBEs and eventually to the disappearance of SBEs. Increasing synaptic strengths leads to high activity rate, eventually obtaining the merger of SBEs into a tonic firing mode.

The time constant of the dynamic thresholds τ_{th} provides further flexibility in adjusting ΔISI to experimental data. An example is shown in Figure 6, where we compare our model to a specific experiment, obtaining a good fit to a Lévy distribution almost up to 1000 msec. In fact, the increase of τ_{th} allowed us to increase the domain over which the Lévy distribution is valid from 100 to 1000 msec.

5.2 Self-Consistency. Using experimental data, we can test the model. We feed a simulated neuron with spike sequences of the experimental neurons via frequency-dependent synapses while removing the external input. We have data of 36 real neurons and arbitrarily label 32 of them as excitatory presynaptic neurons and 4 as inhibitory ones. We expect the simulated neuron to be synchronized with the network activity, that is, to spike mainly within SBEs. The question to be tested is whether the distribution of its output spike train will match the experimental one (average of all experimental neurons). The results indicate that the model is consistent with the experimental activity. When a simulated neuron receives a Lévy distributed

stimulus, it responds with a Lévy distributed pattern of activity. The exact pattern is determined mainly by the choice of synaptic strengths. There are only slight differences between the response of an IF neuron with a fixed threshold and an IF neuron with a dynamic threshold given our set of parameters.

In some experimental preparations, we notice that there are few neurons that have much higher firing rates than others. It would be interesting to find the character of these neurons—In particular, to understand if they are inhibitory neurons, whose role is to regulate the activity of the network, or excitatory ones, reacting to the changing environment. An experimental method to answer this question can be suggested on the basis of our model. The real neurons can be stimulated electrically through the electrode they are attached to. One can inject positive currents to one of the neurons, causing it to spike intensively. The specific balance in our simulated network enables a higher firing rate for inhibitory neurons than for excitatory neurons. This could be tested. Injecting an excitatory neuron with positive currents, thus making it permanently active, we find in our model that this is sufficient to induce permanent activity in any inhibitory neuron connected to that excitatory neuron but not in any other excitatory neuron. This is demonstrated in Figure 7. It can be used as a basis for mapping out inhibitory neurons in the experimental preparation. It also suggests that the observed spiking neurons in the (unstimulated) preparation are inhibitory neurons whose activity may regulate the system.

6 Discussion

From the results of section 4, we conclude that inhomogeneities in neural parameters lead to correct behavior of the neuronal activity: (1) time-varying external currents lead to the rising spatiotemporal profile of a SBE; (2) inhomogeneity in the resistances leads to the detailed structure of a SBE; (3) the accurate distribution of spikes is obtained using dynamic thresholds; and (4) Lévy distribution of SBEs is also obtained due to inhomogeneity in the system.

Dynamic thresholds are often used to account for neuronal adaptation through their increase. In the model of section 4, we have employed two types of neurons, which have both increasing and decreasing dynamical thresholds. This observation is consistent with known biological observations of a large firing repertoire of neurons (Meunier & Segev, 2001). Moreover, a recent study of interneurons (Markram, 2003) reported the existence of many types of inhibitory neurons, each having its own characteristic electrical response to stimulus.

It was suggested a long time ago (Gerstein & Mandelbrot, 1964) that if the membrane voltage has a random walk behavior, one can obtain many heavy-tailed distributions. Dynamic thresholds of the kind we use impose a random walk-like behavior on the membrane voltage and were neces-

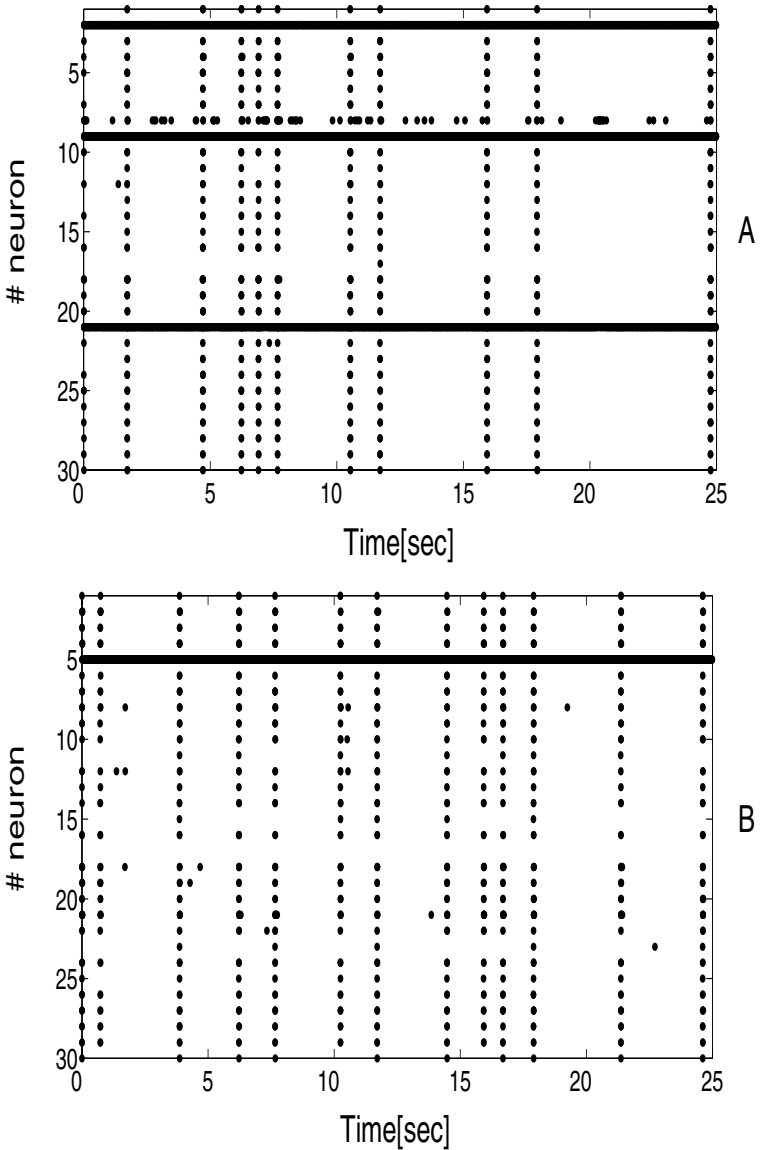


Figure 7: Response of the model to external stimulations. (Top) Positive external current is injected to an excitatory neuron (number 9). The target inhibitory neurons 2 and 21 respond with continuous spiking. Target neuron 8 is also inhibitory and shows extensive spiking outside SBEs. The rest are excitatory neurons that spike only within SBEs. (Bottom) Positive external current is injected to an excitatory neuron (number 5) that does not have any inhibitory neurons as targets. Hence, no other neurons exhibit continuous spiking behavior.

sary to obtain the distributions observed experimentally, so our results embrace their suggestion. To reinforce this claim, we also examined nonlinear one-dimensional models of neurons, which describe more accurately the changes in the membrane voltage. Using these models in the absence of dynamic thresholds did not lead to better results. However, using a two-dimensional model that endows its membrane with a more complicated response by making partial use of ionic channel dynamics can explain the neuronal distributions we see in the experiments (Volman, Baruchi, Persi, & Ben-Jacob, 2004).

The variance of the heavy-tailed distributions of ΔISI diverges. This may imply that the system we study has the potential to operate on many different timescales. This flexibility is important to allow different neuronal networks, with different functional roles, to be responsive to different timescales depending on the specific inputs they have to process. Therefore, in a case of processing a given task (or stimulation), we would expect to observe changes in the shape and variability of the discussed distributions. It will be interesting to understand which features of the stimulation will be coded by the individual neurons and which features (if any) will be coded on the whole network level. This will be tested in the future.

An important open problem is to understand why networks of different sizes behave similarly. We believe that this can be understood by invoking the concept of neural regulation (Horn, Levy & Ruppin, 1998) or synaptic scaling (Turrigiano, Leslie, Desai, Rutherford, & Nelson, 1998; Abbott & Nelson, 2000). Preliminary studies show this to be the case, but it requires further investigation.

Appendix

Parameters of simulation in (Tsodyks et al., 1999): 400 excitatory neurons and 100 inhibitory neurons. Reset and threshold membrane potentials: $V_{reset} = 13.5$ and $V_{threshold} = 15$. Resistances are 1. External currents were driven from a unit distribution centered at the threshold level with a range of 5% of the threshold. Time constants of the neurons: $\tau_{mem} = 30$ msec, refractory period of 2 and 3 msec for inhibitory and excitatory neurons, respectively. Synaptic parameters were taken from gaussian distributions. Standard deviations are half of the following average values (with cutoffs of 2·average and 0.2·average): $A(ee) = 1.8$, $A(ei) = 5.4$, $A(ie) = A(ii) = 7.2$. Average values of utilization: $U(ee) = U(ei) = 0.5$, $U(ie) = U(ii) = 0.04$. Average time constants: $\tau_{rec}(ie) = \tau_{rec}(ii) = 100$ msec, $\tau_{rec}(ee) = \tau_{rec}(ei) = 800$ msec, $\tau_{fac}(ie) = \tau_{fac}(ii) = 1000$ msec. Fixed time constant of $\tau_{ina} = 3$ msec. It is reported that the results of this simulation are robust under changes of up to 50% in the average values.

Parameters of our model: 27 excitatory neurons and 3 inhibitory neurons. Reset and threshold membrane potentials: $V_{reset} = 0$ and $V_{threshold} = 1$. Resistances to synaptic currents $\sim U(0.1, 0.4)$. Resistance to external currents

remains 1. External currents $\sim N(0.86, 0.15)$. Time constants of the neurons: $\tau_{mem} \sim U(9.5, 10.5)$ msec, refractory periods $\sim U(2, 3)$ msec for all neurons. Fixed time constant of $\tau_{ina} = 10$ msec. All other parameters are unchanged.

Acknowledgments

This work was supported by a research grant of the Israel Science Foundation.

References

- Abbott, L. F., & Nelson, S. B., (2000). Synaptic plasticity: Taming the beast. *Nature Neuroscience Supplement*, *3*, 1178–1183.
- Brandman, R., & Nelson, M. E. (2002). A simple model of long-term spike train regularization. *Neural Computation*, *14*, 1575–1597.
- Gerstein, G., & Mandelbrot, B. (1964). Random walk models for the spike activity of single neuron. *Biophysical Journal*, *4*, 41–68.
- Horn, D., Levy, N., & Ruppin, E. (1998). Memory maintenance via neuronal regulation. *Neural Computation*, *10*, 1–18.
- Horn, D., & Opher, I. (2000). Complex dynamics of neuronal thresholds. *Neurocomputing*, *32*, 161–166.
- Horn, D., & Usher M. (1989). Neural networks with dynamical thresholds. *Phys. Rev.*, *A40*, 1036–1044.
- Mantegna, R. N., & Stanley, H. E. (1995). Scaling behaviour in the dynamics of an economic index. *Nature*, *376*, 46–49.
- Markram, H. (2003). *Molecular determinants of neuronal diversity*. Lecture at the Brain in Motion symposium, Lausanne.
- Markram, H., Pikus, D., Gupta, A., & Tsodyks, M. (1998). Potential for multiple mechanisms, phenomena and algorithms for synaptic plasticity at single synapses. *Neuropharmacology*, *37*, 489–500.
- Markram, H., & Tsodyks M. (1996). Redistribution of synaptic efficacy between neocortical pyramidal neurons. *Nature*, *382*, 807–810.
- Marom, S., & Shahaf, G. (2002). Development, learning and memory in large random networks of cortical neurons: Lessons beyond anatomy. *Quarterly Rev. Biophysics*, *35*, 63–87.
- Meunier, C., & Segev, I. (2001). Neurons as physical objects: Structure, dynamics and function. In F. Moss & S. Gielen (Eds.), *Handbook of Biological Physics*, (Vol. 4, pp. 353–466). Dordrecht: Elsevier.
- Nolan, J. P. (1998). Parameterization and modes of stable distribution. *Statistics and Probability Letters*, *38*, 187–195.
- Nolan, J. P. (2001). Maximum likelihood estimation and diagnostics for stable distributions. In O. E. Barndorff-Nielsen, T. Mikosch, & S. I. Resnick (Eds.), *Lévy processes: Theory and applications*. Boston: Birkhäuser.
- Nolan, J. P. (2004). *Stable distributions—models for heavy-tailed data*. Boston: Birkhäuser.

- Peng, C. K., Mietus, J., Hausdorff, J. M., Havlin, S., Stanley, H. E., & Goldberger, A. L. (1993). Long-range anticorrelations and non-gaussian behavior of the heartbeat. *Phys. Rev. Lett.*, *70*, 1343–1346.
- Segev R. (2002). *Self-organization of in vitro neuronal networks*. Unpublished doctoral dissertation, Tel-Aviv University.
- Segev, R., Benveniste, M., Shapira, Y., Hulata, E., Cohen, N., Palevski, A., Kapon, E., & Ben-Jacob E. (2001). Long-term behavior of lithographically prepared in vitro neural network. *Physical Review Lett.*, *88*, 118102.
- Segev, R., Shapira, Y., Benveniste, M., & Ben-Jacob E. (2001). Observation and modeling of synchronized bursting in two-dimensional neural network *Physical Review E.*, *64*, 011920.
- Shahaf, G., & Marom, S. (2001). Learning in networks of cortical neurons. *Journal of Neuroscience*, *21*, 8782–8788.
- Tsodyks, M., Pawelzik, K., & Markram H. (1998). Neural networks with dynamic synapses. *Neural Computation*, *10*, 821–835.
- Tsodyks, M., Uziel, A., & Markram, H. (1999). Synchrony generation in recurrent networks with frequency-dependent synapses. *Journal of Neuroscience*, *20*, RC50 1–5.
- Turrigiano, G., Leslie, K., Desai, N., Rutherford, L., & Nelson, S. (1998). Activity-dependent scaling of quantal amplitude in neocortical neurons. *Nature*, *391*, 892–895.
- Volman, V., Baruchi, I., Persi, E., & Ben-Jacob, E. (2004). Generative modelling of regulated dynamical behavior in cultured neuronal networks. *Physica A*, *335*, 249–278.
- Ying-Hui, L., & Wang, X. J. (2000). Spike-frequency adaptation of generalized leaky integrate and fire model neuron. *Journal of Computational Neuroscience* *10*, 25–45.

Received July 30, 2003; accepted May 21, 2004.